DOI 10.14622/Advances_48_2022_08

Creation of a comprehensive high-resolution image data set on an industrial web press to investigate hydrodynamic pattern formation in gravure printing

Pauline Brumm[1,2], Thomas Sprinzing[3], Thorsten Euler[1], Matthias Galus[3], Armin Weichmann[3] and Edgar Dörsam[1,2]

[1] Technical University of Darmstadt, Department of Mechanical Engineering, Institute of Printing Science and Technology, Magdalenenstr. 2, 64289 Darmstadt, Germany

[2] Collaborative Research Center (CRC) 1194 – Interaction between Transport and Wetting Processes, Project C01, Germany

[3] Hochschule der Medien Stuttgart, Institut für Angewandte Forschung (IAF), Nobelstr. 10, 70569 Stuttgart, Germany

E-mails: brumm@idd.tu-darmstadt.de; sprinzing@hdm-stuttgart.de; euler@idd.tu-darmstadt.de; galus@hdm-stuttgart.de; weichmann@hdm-stuttgart.de; doersam@idd.tu-darmstadt.de

Short abstract

Hydrodynamic pattern formation in gravure printing is not yet fully understood, but a deep insight into the fluid transfer process is crucial for process control and for high-quality printed layers. Therefore, a large-scale gravure printing trial was conducted on an industrial-scale web press to analyze pattern formation phenomena on the printed samples using various complementary methods: deep learning for pattern classification, Fourier analysis of ribbing patterns, gradation measurements, mottle index measurements and missing dots analysis. The printing form layout was especially developed for use with these analyzing methods. From over 23 km of printed foil and paper, over 4 000 printed sheets were extracted and cut into pieces, from which over 1 200 were scanned at a resolution of 2 400 dpi (10.58 µm per pixel), resulting in images of size 20 400 × 28 080 pixels. Thus, a comprehensive, versatile high-resolution image data set larger than three terabytes was created which can be used to investigate the influence of printing parameters on pattern formation. During the printing trial, the following printing parameters were varied systematically: printing velocity (15–240 m/min), type of ink (solvent-based, water-based), ink viscosity (base, high, medium, low), type of substrate (foil, paper), electrostatic assist (ESA) (on, off) and doctor blade angle (high, medium, low). First analysis results are presented in this article.

Keywords: rotogravure, fluid transfer, ink splitting, parameter study, quality control, dynamic wetting

1. Introduction and background

Understanding hydrodynamic pattern formation during fluid transfer in gravure printing is crucial for the fabrication of homogeneous ultra-thin functional layers as e.g. used in printed electronics, for large-throughput high-quality graphical printing applications, as well as for special applications like printed security features or biomedical printing. Numerous researchers like Kunz (1975), Hübner (1991), Kumar (2015), Grau, et al. (2016) and Schäfer, et al. (2019) have contributed to a deeper understanding of fluid transfer in gravure printing in the last decades. However, pattern formation dynamics are still only partially understood and the printing industry often relies on the practical experience of professional printers. Therefore, the aim of our large-scale gravure printing trial was to systematically investigate the influence of selected major printing parameters (printing velocity, type of ink, ink viscosity, type of substrate, electrostatic assist (ESA) and doctor blade angle) on hydrodynamic pattern formation. Various pattern formation phenomena can be observed in the dried ink layer, such as (missing) dots, ribbing and more complex patterns (Brumm, et al., 2021a). Depending on the printing application, a certain pattern is desired or even required. For halftones in graphical applications, typically dot patterns are desired, whereas for functional coatings or printed electronics, closed homogeneous layers of ink with the least amount of pattern formation possible are generally needed.

2. Materials and methods

2.1 Gravure printing trial

2.1.1 Design of experiments

We conducted a 3-day printing trial on an industrial-scale gravure printing machine Bobst Rotomec MW 60 (Bobst, Mex, Switzerland) with a printing form cylinder of 700 mm circumference and 700 mm face and a maximum printing speed of 300 m/min. On day one we printed with solvent-based ink (NC 133-15, magenta, Siegwerk, Siegburg, Germany) on foil (WSS 20 BoPP solid white film, both sides heat sealable, treated, Taghleef Industries, Dubai, United Arab Emirates), on day two with solvent-based ink (NC TOB, magenta, Siegwerk, Siegburg, Germany) on two different paper substrates (UPM Smart G 60 g/m^2, super-calendered, UPM, Augsburg, Germany and Sigmakraft RTC Green 70 g/m^2, coated, Mosaico Specialty Papers, Altavilla Vicentina, Italy) and on the third day with water-based ink (R0001235761, red bluish, Sun Chemical, Niedernhausen, Germany) again on the Sigmakraft paper.

The design of experiments is based on ascending velocity ramps with the printing velocities 15, 30, 60, 90, 120, 180, and 240 m/min as target velocities. ESA was always turned off for 15 and 30 m/min and was turned both off and on for the other printing velocities. Furthermore, the ink viscosity and the angle of the doctor blade (Swedcut MicroKote G, RG10530, coated carbon steel blade, 40 mm × 0.15 mm Standard Lamella, Swedev, Munkfors, Sweden) were varied in three steps (high, medium, low). The water-based ink was even prepared using four different viscosities (base, high, medium, low). For diluting the solvent-based inks, a nearly azeotropic mixture of ethanol (30 %) and ethyl acetate (70 %) was used. The water-based ink was diluted with tab water. The ambient temperature and humidity were recorded and the ink temperature was monitored during the printing trial. Printing ink viscosity was measured with a 4 mm ISO flow cup (DIN EN ISO 2431) as well as a 4 mm DIN flow cup (DIN 53211) (Deutsches Institut für Normung, 2019; 1987) and was controlled with a Fasnacht Viscopoint IL CPS viscosity sensor in combination with a viscosity control system Fasnacht pentasmart (Fasnacht Dynamics AG, Worb, Switzerland). After the printing trial, ink viscosities were measured using a rotational rheometer Kinexus Lab+ (NETZSCH-Gerätebau GmbH, Selb, Germany). Doctor blade pressure (1.5 bar), impression roller pressure (1.5 bar) as well as impression roller hardness (80 Shore A) were kept constant. In total, 17 velocity ramps were performed with 12 parameter combinations each. For each parameter combination, 20 sheets (each 600 mm × 700 mm) were manually cut out, which results in over 4 000 sheets in total. The sheets were post-processed according to the chosen analyzing method which mostly required further cutting as well as digitization steps.

2.1.2 Printing form layout

We used an electromechanically engraved, chrome-plated printing form (circumference 700 mm, engraving width 590 mm, pyramid shaped cells). The printing form was engraved on a Hell K500 engraving system (Hell Gravure Systems GmbH & Co. KG, Kiel, Germany). Several raster angles (Hell engraving angles 0, 2, 4), raster frequencies (60, 70, 80, 100 lines/cm) and tonal values (0, 1, 2, 3, 4, 5, 8, 10, 15, 20, 25, 30, 35, 40, 45, 50, 55, 60, 65, 70, 75, 80, 85, 90, 93, 95, 98, 100 %) were realized on the same printing form with constant stylus angle 120°. Hell engraving angles 0 (2, 4) equal a raster angle of 36.87° (59.35°, 40.16°). The printing form layout was especially developed for use with the analyzing methods as described in Section 2.3. Five defined parts (A, B, C, D, E) of the printing form layout are directly dedicated to the five different analyzing methods, see Figure 1. Part A is especially used for classification of patterns with deep learning, part B for Fourier analysis of ribbing patterns, part C for gradation measurements, part D for mottle index measurements and part E for missing dots analysis. In Figure 1 in part C, D and E, Hell engraving angle 0 is displayed as cyan and Hell engraving angle 4 as black, both with a nominal raster frequency of 80 lines/cm. In part A and B, where the raster angle is always Hell engraving angle 2, the color black stands for a nominal raster frequency of 60 lines/cm, yellow for 70 lines/cm, magenta for 80 lines/cm and cyan for 100 lines/cm.

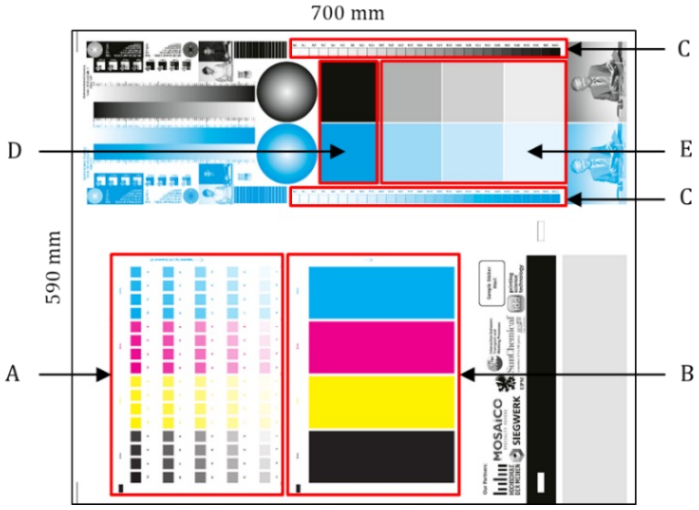

Figure 1: Printing form layout: part A is used for classification of patterns with deep learning, part B for Fourier analysis of ribbing patterns, part C for gradation measurements, part D for mottle index measurements and part E for missing dots analysis

2.2 Sample digitization and post-processing

Parts A and B of the printing form layout (Figure 1) were digitized using two Epson Perfection V850 Pro flatbed scanners (Seiko Epson Corporation, Suwa, Japan) operated with the professional scanning software Silverfast Ai Studio 9 (LaserSoft Imaging AG, Kiel, Germany). The scanner was color-calibrated before each use with a reflected light Kodak IT8-Target. The nominal scanning resolution was chosen as 2 400 dpi (10.58 µm per pixel) and the scanned images were saved as uncompressed TIF files with 16-bit lightness values per R, G and B color channel. All filters and retouching options were turned off. In total, over 1 200 images of size 20 400 × 28 080 pixels were scanned. For further processing of the scanned images, a source code in the programming language Python was developed which automatically identifies and cuts out the 13 mm × 13 mm squares in part A and the 64 mm × 179 mm rectangles in part B. This leads to over 48 000 cut-out squares and over 2 400 cut-out rectangles. Parts D and E were scanned together with an Epson Perfection 4870 Photo flatbed scanner (Seiko Epson Corporation, Suwa, Japan) at a nominal resolution of 1 200 dpi (21.17 µm per pixel) in 8-bit grayscale. The scanner was calibrated that the brightest substrate delivered lightness values above 240 but less than 255 (no overexposure) and the darkest patch, the solid black patch of area D, had values between 5 and 50.

2.3 Sample analysis

2.3.1 Classification of patterns with deep learning

The cut-out squares that were derived from part A after post-processing shall be classified using trained convolutional neural networks (CNNs) from Brumm, et al. (2021b), a common method in deep learning. These CNNs were trained to distinguish between three classes of pattern formation: dots, fingers and mixed. Fingers are also known as 'ribbing' patterns and derive from Saffman-Taylor instabilities at the ink-air-interface (Saffman and Taylor, 1958). The classified images shall be used to create regime maps, see Brumm, et al. (2021a), in which two or more printing parameters are displayed on the axes, e.g., printing velocity and tonal value, and data points including the pattern class are plotted. Regime maps visualize the cause-effect-correlations between printing parameters and printed pattern class and shall help the operators of a printing press to choose the correct set of printing parameters for their intended application. We assume that these regime maps are especially useful for developing innovative printed products, for operating the printing press at uncommon process parameters and for process scaling.

2.3.2 Fourier analysis of ribbing patterns

The cut-out rectangles from part B shall be analyzed with a 1-dimensional fast Fourier transformation algorithm in the programming language Matlab which was developed and already approved for the analysis of ribbing patterns in flexographic printing by Brumm, Sauer and Dörsam (2019). The Fourier analysis yields dominant frequencies of the ribbing patterns which are plotted in double-logarithmic scale over printing velocity. From the plots, scaling behavior of pattern formation in form of scaling exponents can be extracted. These scaling exponents help the operator of the printing press to tune the printing parameters in order to obtain a certain ribbing pattern, e.g., for the fabrication of capillary networks for biomedical applications (Fritschen, et al., 2021), or to reduce the ribbing pattern as much as possible as it is mostly the case in graphical printing and printed electronics.

2.3.3 Gradation measurements

Gradation measurements shall be performed on the tonal value wedges over the whole tonal range (28 steps, see Section 2.1.2) in part C of the printing form layout. The spectral values will be measured by a Techkon SpectroDens spectro-densitometer (TECHKON GmbH, Königstein im Taunus, Germany), converted into CIE *L*a*b** values and then the spot color tonal values (SCTV) (according to ISO 20654:2017) will be calculated and evaluated (International Organization for Standardization, 2017).

2.3.4 Mottle index measurements

Mottle index measurements shall be performed on the two 100 % tonal value fields in part D. The overall mottle index is determined within a 300 dpi grid calculated by downscaling the 1 200 dpi image. The evaluation program is written in Java by Weichmann (2015) basically using the algorithm by Rosenberger (2002). It works on an area of 512 x 512 pixels (43.34 mm × 43.34 mm), calculates the mean of the absolute differences of the mean of the gray values of the four sub-squares in a circumscribing square, takes the standard deviation of these means of all squares in the area multiplied by the mean of the grey values of the squares multiplied by the standard deviation of the mean of the grey values of the squares. The size of the squares increases over eight steps: 85, 170, 340, 680 µm, 1.34, 2.68, 5.42, 10.84 mm. The values for the different sizes show the inhomogeneity of the solid ink layer in the respective space frequency areas. It can be assumed that some of these correlates better to the finger structures than others, because of the pattern of the fingers being of similar size to these squares. The final mottle index is the mean of the eight values. The greater the value the more mottle is detected. An overall mottle index greater than 10 indicates well visible structures. Even lower numbers are associated with mottle, however, less visible.

2.3.5 Missing dots analysis

In part C, the tonal values of 75 %, 50 % and 25 % in two Hell engraving angles shall be used to count the missing dots per area. The evaluation program is written in Java by Weichmann (2015) and works with the 1 200 dpi images. It utilizes edge filtering and adaptive dot size filtering to count the number of missing dots in these fields and normalize them to $1/cm^2$. As missing dots distort the image and decrease the image quality, the less missing dots the better.

3. Results and discussion

3.1 Printing trial protocol

In total, we consumed over 23 km of foil and paper for printing. We extracted over 4 000 printed sheets from the printed rolls. The printing trial without preparatory work but including subsequent cutting of the sheets from the printed rolls took over 140 hours. The sorting, labeling and cutting of the sheets into smaller pieces consumed over 200 hours and over 350 hours were needed for scanning of over 1 200 images of only part A and B of the samples.

3.2 Data set characteristics

To the best of our knowledge, our high-resolution image data set is by far the largest industrial-scale scientific data set for gravure printing compared with earlier studies. The over 1 200 scanned images of part A and B alone provide high-quality uncompressed image data of gravure printed patterns with a total size of over three terabytes. If applicable, the cut-out rectangles and squares can be saved in a compressed and downscaled data format during post-processing to save memory capacity. The scanned images of part D and E will provide another several gigabytes of image data. The data set helps to gain a deeper understanding of pattern formation in gravure printing.

Cut-outs from two exemplary samples are shown in Figure 2. Sample #1 (identification number: B2-03_ECPvmam_V240_ESA1) was printed at 240 m/min on the Sigmakraft paper with the NC TOB ink of medium viscosity (20 s with ISO flow cup) with ESA turned on and medium blade angle of nominal 55°. Sample #2 (B3-05_WCPvlam_V015_ESA0) was printed at 15 m/min, on Sigmakraft paper with water-based ink of low viscosity (17 s with ISO flow cup) with ESA turned off and medium blade angle 55°.

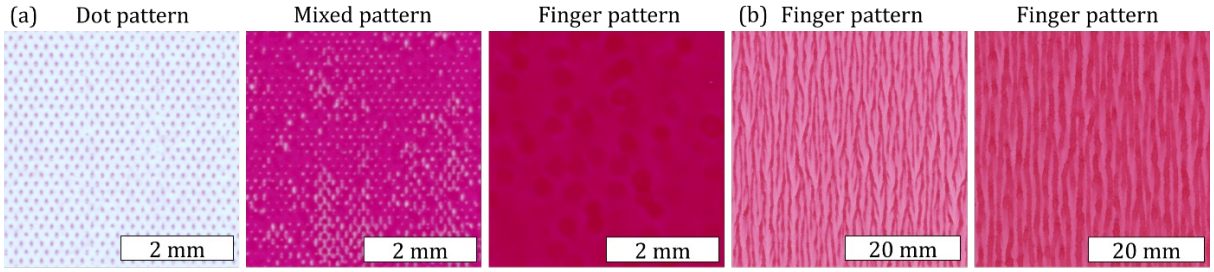

Figure 2: Exemplary cut-outs from samples #1 (a) and #2 (b) show various types of patterns

3.3 First analysis results of pattern formation

For sample #1, we calculated the spot color tonal values (SCTV) and plotted them over the tonal value from the data for Hell engraving angle 0 and 4, see Figure 3a. The curves of the two Hell engraving angles differ slightly but are both relatively close to a linear curve with a slope of 1, which would be the ideal behavior. For sample #2, we observed strong finger patterns (Figure 2b), which we analyzed using the Fourier analysis approach. Figure 3b shows four Fourier spectra for the four different raster frequencies. The global peaks at frequencies around 5 cm^{-1} to 7 cm^{-1} reveal the dominant frequencies of the ribbing patterns, which are much lower than the underlying raster frequencies of 60 cm^{-1} to 100 cm^{-1} measured along the raster angle. The raster frequency is visible in the right half of the Fourier spectra in form of small local sharp peaks at 55 cm^{-1}, 65 cm^{-1}, 75 cm^{-1} and 94 cm^{-1} since the Fourier analysis is performed perpendicular to the printing direction and not along the raster angle. In conclusion, the ribbing patterns span 11 to 13 raster dots on average and thus are clearly visible to the human observer as printing defects.

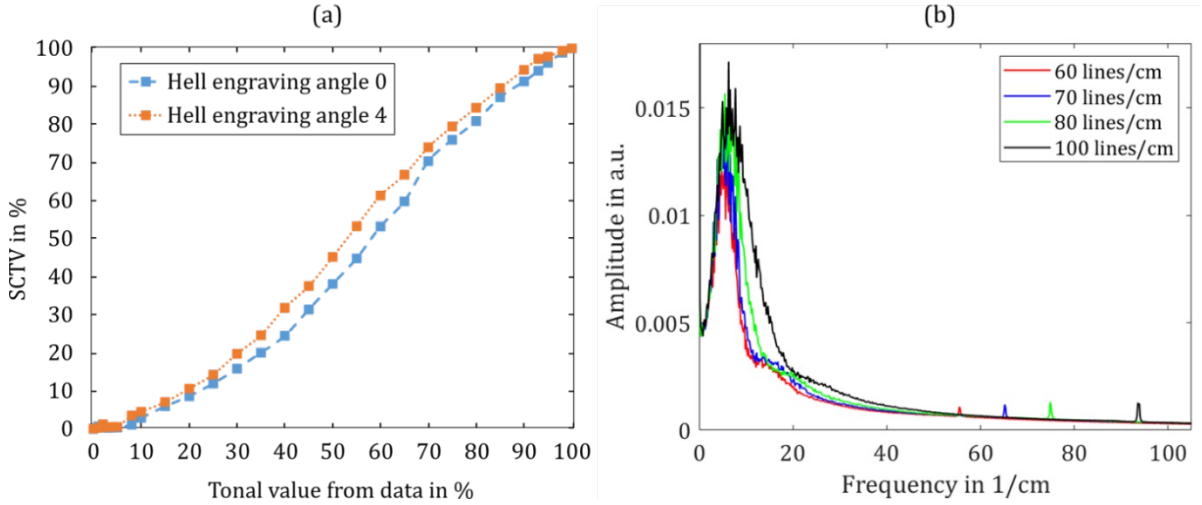

Figure 3: Exemplary SCTV curves for two Hell engraving angles for sample #1 (a) and exemplary Fourier spectra for four raster frequencies at Hell engraving angle 2 for sample #2 (b)

Exemplary mottle index measurements can be found in Table 1 and an exemplary missing dots analysis is depicted in Table 2.

Table 1: Exemplary mottle index measurements for sample #1 for two Hell engraving angles

Hell engraving angle	Mottle 1	Mottle 2	Mottle 3	Mottle 4	Mottle 5	Mottle 6	Mottle 7	Mottle 8	Mottle index
0	143.970	98.434	16.344	1.603	0.207	0.043	0.012	0.015	32.579
4	56.479	29.139	4.821	0.865	0.220	0.115	0.204	0.138	11.498

Table 2: Exemplary missing dots analysis for sample #1 for two Hell engraving angles

Hell engraving angle	0			4		
Tonal value	25 %	50 %	75 %	25 %	50 %	75 %
Missing dots per cm^2	1 228.0	3.2	8.5	4 836.0	191.0	257.0

Based on visual evaluation, the image quality of our high-resolution data set is very satisfactory for pattern analysis. Further evaluations are currently being carried out.

4. Conclusions and outlook

We were able to create a comprehensive, high-resolution image data set and showed first exemplary results of the pattern formation analysis. Further analyzing methods can be applied to the printed samples or the data set. At this point we would like to emphasize the versatility of the data set, which we plan to make available to the public under creative commons license and use as a benchmark for the comparison between classical electromechanically engraved printing forms and recently developed polymeric printing forms. Besides, we plan to compare pattern formation phenomena and their scaling behavior as observed on different printing machines. Another future investigation shall be focused on the correlation of mottle index and ribbing pattern frequency.

Acknowledgements

We kindly acknowledge the financial support by the Deutsche Forschungsgemeinschaft (DFG, German Research Foundation) – Project-ID 265191195 – SFB 1194 'Interaction between Transport and Wetting Processes', project C01. We kindly thank CAPA Crummenerl & Albers and UPM for providing paper substrates and Siegwerk and Sun Chemical for providing printing inks.

References

Brumm, P., Sauer, H.M. and Dörsam, E., 2019. Scaling behavior of pattern formation in the flexographic ink splitting process. *Colloids and Interfaces*, 3(1): 37. https://doi.org/10.3390/colloids3010037.

Brumm, P., Weber, T.E., Sauer, H.M. and Dörsam, E., 2021a. Ink splitting in gravure printing: localization of the transition from dots to fingers. *Journal of Print and Media Technology Research*, 10(2), pp. 81–93. https://doi.org/10.14622/JPMTR-2016.

Brumm, P., Lindner, N., Weber, T.E., Sauer, H.M. and Dörsam, E., 2021b. A deep learning approach for the classification task of gravure printed patterns. In: C. Ridgway, ed. *Advances in Printing and Media Technology: Proceedings of the 47th International Research Conference of Iarigai.* Athens, Greece, 19–23 September 2021, pp. 2–9. Darmstadt: iarigai. https://doi.org/10.14622/Advances_47_2021.

Deutsches Institut für Normung, 2019. *DIN EN ISO 2431 Paints and varnishes – Determination of flow time by use of flow cups (ISO 2431:2019, Corrected version 2019-09*). Berlin: DIN.

Deutsches Institut für Normung, 1987. *DIN 53211 Paints, varnishes and similar coating materials: Determination of flow time using the DIN flow cup*. Berlin: DIN.

Fritschen, A., Brumm, P., Doss, L., Dörsam, E. and Blaeser, A., 2021. Fabrication of vascular network mimicking pattern using flexographic printing technology. In: *TERMIS 6th World Congress*. Maastricht, the Netherlands, November 15–19, 2021.

Grau, G., Cen, J., Kang, H., Kitsomboonloha, R., Scheideler, W.J. and Subramanian, V., 2016. Gravure-printed electronics: recent progress in tooling development, understanding of printing physics, and realization of printed devices. *Flexible and Printed Electronics*, 1(2): 023002. https://doi.org/10.1088/2058-8585/1/2/023002.

Hübner, G., 1991. *Ein Beitrag zum Problem der Flüssigkeitsspaltung in der Drucktechnik.* Dr.-Ing. Dissertation. Technische Hochschule Darmstadt. https://doi.org/10.25534/tuprints-00013550.

International Organization for Standardization, 2017. *ISO 20654:2017 Graphic technology – Measurement and calculation of spot colour tone value*. Geneva: ISO.

Kumar, S., 2015. Liquid transfer in printing processes: liquid bridges with moving contact lines. *Annual Review of Fluid Mechanics*, 47, pp. 67–94. https://doi.org/10.1146/annurev-fluid-010814-014620.

Kunz, W., 1975. Ink transfer in gravure process. In: *TAGA Proceedings 1975: Annual meeting of the Technical Association of the Graphic Arts*. Toronto, Ontario, 1975. Rochester, NY, USA: TAGA, pp. 151–176.

Rosenberger, R.R., 2002. *Mottle measurement of wet trap, back trap and other motley images*. [pdf] VERITY IA. Available at: <https://www.verityia.com/_files/ugd/c4e5fa_efd8667d40f44c45a0187b99b2fb7559.pdf> [Accessed 22 March 2022].

Saffman, P.G. and Taylor, G.I., 1958. The penetration of a fluid into a porous medium or Hele-Shaw cell containing a more viscous liquid. *Proceedings of the Royal Society A: Mathematical, Physical and Engineering Sciences*, 245(1242), pp. 312–329. https://doi.org/10.1098/rspa.1958.0085.

Schäfer, J., Roisman, I.V., Sauer, H.M. and Dörsam, E., 2019. Millisecond fluid pattern formation in the nip of a gravure printing machine. *Colloids and Surfaces A: Physicochemical and Engineering Aspects*, 575, pp. 222–229. https://doi.org/10.1016/j.colsurfa.2019.04.085.

Weichmann, A., 2015. *GravureQ: commercially available software for mottle and missing dots analysis*. Hochschule der Medien Stuttgart, Germany.